

Stent maps – Comparative visualization for the prediction of adverse events of transcatheter aortic valve implantations

Silvia Born, Simon H. Sündermann, Christoph Russ, *Student Member, IEEE*, Raoul Hopf, Carlos E. Ruiz, Volkmar Falk, and Michael Gessat

Abstract— Transcatheter aortic valve implantation (TAVI) is a minimally-invasive method for the treatment of aortic valve stenosis in patients with high surgical risk. Despite the success of TAVI, side effects such as paravalvular leakages can occur postoperatively. The goal of this project is to quantitatively analyze the co-occurrence of this complication and several potential risk factors such as stent shape after implantation, implantation height, amount and distribution of calcifications, and contact forces between stent and surrounding structure. In this paper, we present a two-dimensional visualization (stent maps), which allows (1) to comprehensively display all these aspects from CT data and mechanical simulation results and (2) to compare different datasets to identify patterns that are typical for adverse effects. The area of a stent map represents the surface area of the implanted stent – virtually straightened and uncoiled. Several properties of interest, like radial forces or stent compression, are displayed in this stent map in a heatmap-like fashion. Important anatomical landmarks and calcifications are plotted to show their spatial relation to the stent and possible correlations with the color-coded parameters. To provide comparability, the maps of different patient datasets are spatially adjusted according to a corresponding anatomical landmark. Also, stent maps summarizing the characteristics of different populations (e.g. with or without side effects) can be generated.

Up to this point several interesting patterns have been observed with our technique, which remained hidden when examining the raw CT data or 3D visualizations of the same data. One example are obvious radial force maxima between the right and non-coronary valve leaflet occurring mainly in cases without leakages. These observations confirm the usefulness of our approach and give starting points for new hypotheses and further analyses. Because of its reduced dimensionality, the stent map data is an appropriate input for statistical group evaluation and machine learning methods.

Index Terms—Comparative visualization, medical visualization, vessel flattening, transcatheter aortic valve implantation (TAVI)

1 INTRODUCTION

The aortic valve is located between the left cardiac ventricle and the aorta (see Fig. 1). Its function is to open when the blood is ejected from the ventricle into the aorta during systole and to avoid the back-flow of blood into the ventricle during the remainder of the heart cycle (diastole). Stenosis of the aortic valve, due to calcified and stiffened valve leaflets, is the most common heart valve disease in the western countries. It is problematic for several reasons and needs to be treated (see Sec. 3).

The treatment of choice is the surgical implantation of a prosthetic aortic valve. An alternative to open surgery is a minimally-invasive approach, the *transcatheter aortic valve implantation (TAVI)*, where the pathologically altered valve is not replaced surgically but displaced

towards the aortic wall by an expanded stent containing a prosthetic aortic valve (see Fig. 2c).

Especially for high-risk patients this approach is a valid and reasonable alternative to conventional cardiac surgery. However, postoperatively paravalvular leakages (PVL) may occur. PVL is the backflow of blood between the stent and its surrounding structures into the left cardiac ventricle leading to a volume overload and potential dilation of this heart chamber. Occurrence of PVL has been demonstrated to have relevant impact on the survival of patients treated by TAVI [17].

Clinical science has identified different risk factors and predictors for the onset of PVL after TAVI. These theories consider, e.g., the influence of stent deformation, radial attachment forces, or calcifications (see Sec. 3). What still remains unclear is how important these risk factors are for a specific patient, how they interact and which combination of valve type, size, and position could minimize the risk for PVL. The long-term goal of this project is to improve the preoperative planning of TAVI procedures with biomechanical tools that allow to predict the risk of PVL and other complications for specific cases and support the interventionalist in choosing the most appropriate advancement. For this, we are developing a simulation system, which allows to virtually conduct the aortic valve implantation based on the patient's preoperative CT data and calculate the displacement of tissues and calcifications, the deformation of the stent, and the radial forces between these structures [25].

However, predicting displacements, deformity, and forces remains a fully academic research problem as long as we are not able to actually derive clinically useful information from that data. Useful would be, e.g., an odds ratio for a complication to occur under a given configuration or, one step further, an algorithm that searches for a configuration (e.g., stent type and size and ideal implantation position) that minimizes this odds ratio for a given patient. In order to develop this odds ratio, we need to learn, which parameters or parameter combinations indicate PVL. For this, we analyze postoperative CT data with known outcome as a first step before we can apply our findings to preoperative simulation results in the future. For both use cases, a comprehensive presentation of the high-dimensional anatomical and simulation data is needed.

- Silvia Born is with the University of Zurich, Switzerland, Hybrid Laboratory for Cardiovascular Technologies. E-mail: silvia.born@uzh.ch.
- Simon H. Sündermann is with the University Hospital of Zurich, Switzerland, Division of Cardiovascular Surgery. E-mail: simon.suendermann@usz.ch.
- Christoph Russ is with the Swiss Federal Institute of Technology (ETH) Zurich, Switzerland, Computer Vision Laboratory. E-mail: russc@ethz.ch.
- Raoul Hopf is with the Swiss Federal Institute of Technology (ETH) Zurich, Switzerland, Institute of Mechanical Systems. E-mail: hopf@imes.mavt.ethz.ch.
- Carlos E. Ruiz is with the Lenox Hill Hospital, Structural and Congenital Heart Division. E-mail: cruiz@nshs.edu.
- Volkmar Falk is with the University Hospital of Zurich, Switzerland, Division of Cardiovascular Surgery. E-mail: volkmar.falk@usz.ch.
- Michael Gessat is with the University of Zurich, Switzerland, Hybrid Laboratory for Cardiovascular Technologies and the Swiss Federal Institute of Technology (ETH) Zurich, Switzerland, Computer Vision Laboratory. E-mail: mgessat@ethz.ch.

Manuscript received 31 Mar. 2014; accepted 1 Aug. 2014. Date of publication 11 Aug. 2014; date of current version 9 Nov. 2014.

For information on obtaining reprints of this article, please send e-mail to: tvccg@computer.org.

Digital Object Identifier 10.1109/TVCG.2014.2346459

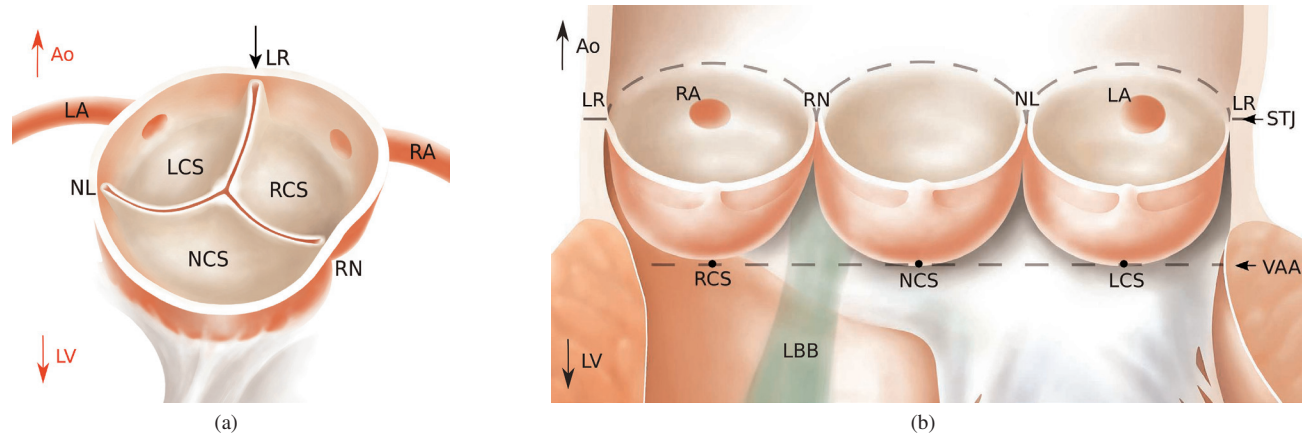


Fig. 1. (a) Healthy tricuspid aortic valve anatomy. (b) Left ventricular outflow tract cut open to show more clearly the three cusps (left coronary, right coronary, non-coronary; named according to the respective ostie located nearby). Abbreviations: Left coronary artery (LA), right coronary artery (RA), left coronary sinus (LCS), right coronary sinus (RCS), non-coronary sinus (NCS), commissure between the respective sinuses (NL, RN, LR), sinotubular junction (STJ), virtual aortic annulus (VAA), left ventricle (LV), aorta (Ao), left bundle branch (LBB).

In this paper, we aim at a visualization approach that incorporates all relevant information and allows users to find patterns indicating PVL. For this, we reduce the dimensionality of the morphological and simulation data and create comprehensive 2D plots. Further, we show how comparison and aggregation of data across individuals in a population or sub-groups of a population can be performed in a straightforward manner. We apply the presented approaches to data from a small cohort of clinical TAVI cases and collect feedback from clinical experts.

2 RELATED WORK

Prediction of TAVI through means of mechanical simulation has been investigated previously – among others – by [3, 6, 25, 30]. They have focused their work on mechanical prediction of stent deployment but have discussed its significance for early detection of PVL and other complications. Lately even a commercial tool has been announced to bring TAVI simulations into the clinics [8]. However, there is still a lack of available methods to evaluate such mechanical simulations and to study and understand the clinical relevance of the produced results for the prediction of potential side effects. Common ways of displaying simulation data are 3D renderings with color-coded radial forces, stress values etc. (see an example in Fig. 3). These visualizations are valid to illustrate specific aspects of single datasets but are inappropriate to efficiently evaluate and compare cases of a larger database. To close this gap, we suggest our stent maps method, which reduces data dimensionality, allows quicker overview and comparison of data, and lays the foundation for a computational evaluation.

Several examples in the medical community demonstrate that methods that reformat and reduce data can lead to useful tools. The learning curve for the user is usually longer for these tools but when established they save time when compared to the examination of raw CT data or 3D scenes. An important example in this context is the bull’s eye plot, which maps the three-dimensional surface of the left cardiac ventricle onto a two-dimensional polar plot. It consists of concentric circles where the innermost circle represents the heart’s apex and the outermost represents the heart base. On these bull’s eye plots 3D image information can be encoded for a quick investigation of the data. This avoids tedious scrolling through 3D image data and decreases intra- and interobserver variability. Nowadays, bull’s eye plots are used in various applications, e.g., in the coronary artery disease diagnostics to compare perfusion of the heart during stress and rest [18, 19] or to analyze strain rate changes (gained from speckle 3D echocardiography) to examine, e.g., ischemia [11]. Termeer et al. proposed a volumetric bull’s eye plot. By adding a third dimension to this plot, the ventricle’s wall thickness can be encoded as additional information [28]. Neugebauer et al. introduced a visualization method where the re-

duction from 3D to 2D helps explore scalar parameters on cerebral aneurysm walls. For this, they combined 3D visualizations of cerebral aneurysms with several 2D maps showing the aneurysm from different view points and provided tools allowing users to correlate between the two depictions [21].

A second group of examples deals with the flattening of tubular anatomical structures. Huysman et al. introduced a generic method to parametrize tubular surfaces onto (flattened) cylinders [15]. Related to this, we also transfer our scene (however consisting of several isolated objects around a common center line) onto a cylinder with generalized cylindrical coordinates. With curved planar reconstruction, e.g., a 3D image dataset is transformed so that a bent vessel is visible in one plane for an easier overview during diagnosis [16, 20]. Flattening is also possible with segmented vessels based on their surface representations [2, 31]. Both methods are especially challenging for bifurcating structures. Ropinski et al. [24] and Diepenbrock et al. [7] used vessel flattening by circular projections for the multimodal, comparative visualization of PET/CT data and Angelelli et al. [1] applied flattening of the aorta to allow for a side-by-side visualization of streamlines from 4D MRI blood flow data. Finally, the flattening of CT colon data was developed to help clinicians find polyps [5, 13].

Along these lines, we apply a novel flattening and reduction approach to multimodal data of the aortic valve and the prosthesis.

3 MEDICAL BACKGROUND

3.1 Aortic valve anatomy

The aortic valve is located in the aortic root at the border between the left cardiac ventricle (LV) and the aorta. It separates the blood pools of these two structures and opens during systole when blood is ejected from the LV into the aorta. The valve is tricuspid, which means that it consists of three semilunar leaflets (cusps) as shown in Figure 1a. The *commissures* mark the border between the three leaflets of the aortic valve and the three sinuses. The right coronary artery (RA) and the left coronary artery (LA), which supply the heart muscle with blood, originate from the corresponding sinuses (right coronary sinus, RCS; left coronary sinus, LCS). One sinus does not contain a coronary artery exit and is called non-coronary sinus (NCS). In this paper, LCS, RCS, and NCS describe the lowest points of the corresponding sinuses (black points in Fig. 1b). The plane defined by these three landmarks is the *virtual aortic annulus* (VAA) whereas the plane defined by the three commissures is called *sinotubular junction* (STJ). These two planes together with the border of the sinuses connecting the commissures and the lowest points of the sinuses is shaped like a crown. Figure 1b shows the anatomical situation of the aortic valve when cut open at the commissure between left and right coronary sinus (LR-

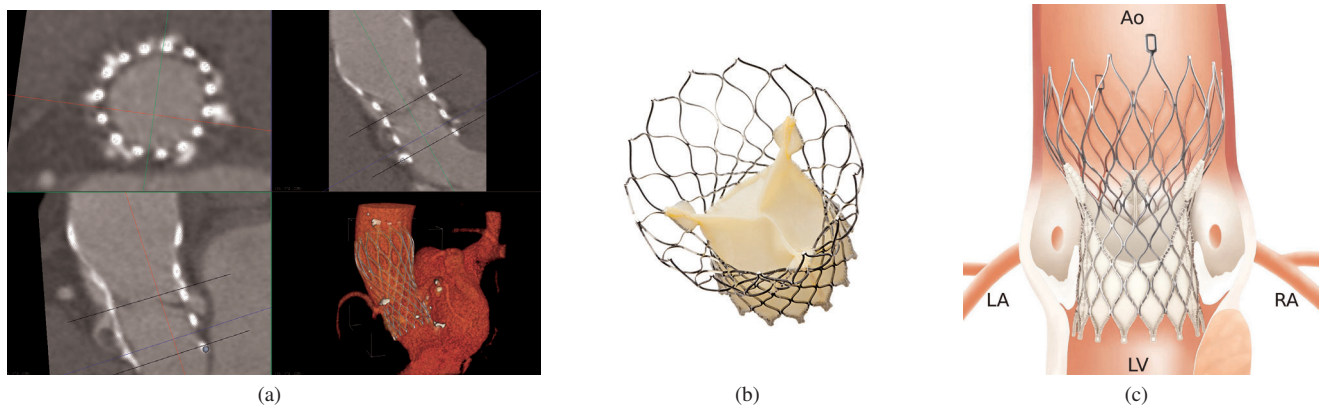


Fig. 2. (a) Postoperative CT data showing the inserted stent as cross-section and longitudinal section in the 2D slices and in a 3D volume rendering. (b) Self-expandable stent as used in the TAVI cases of this paper. The stent contains a tricuspid prosthetic aortic valve made of porcine tissue. The interventionalist can choose from four diameters (23 mm, 26 mm, 29 mm, or 31 mm) depending on the patient's aortic root size. (c) A correctly positioned CoreValve stent in the aortic root (usually the stent is more deformed). Both, a very high and a very low implantation height is suspected to cause leakages. Abbreviations: Left coronary artery (LA), right coronary artery (RA), left ventricle (LV), aorta (Ao).

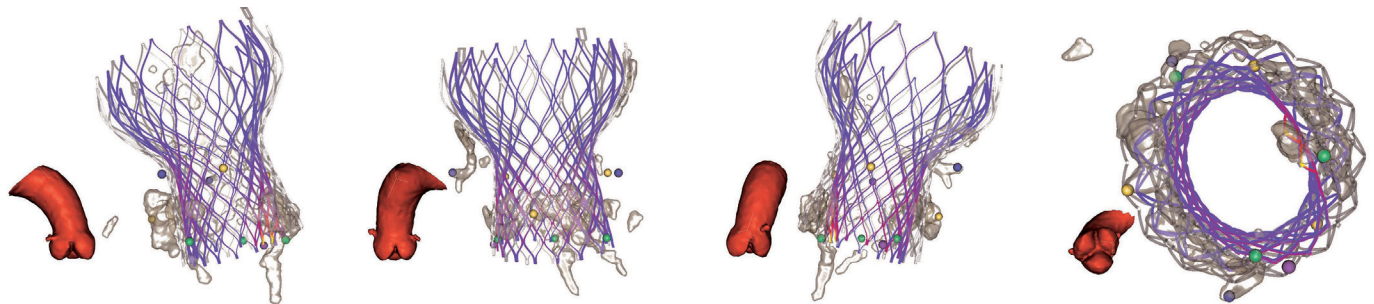


Fig. 3. Conventional visualization of the data in Figure 5b, shows the implanted stent (with radial forces overlay), original stent (gray), calcium (transparent gray), and landmarks (commissures in yellow, sinuses in green, coronary arteries in blue). The first three images show views directed on the commissures (from left to right: NL-commissure, LR-commissure, RN-commissure) and the VAA plane kept horizontally (i.e. sinuses are always displayed in one line). The right image presents the view from below on the VAA plane.

commissure; the other commissures are named RN-commissure and NL-commissure accordingly). This is the view that we have chosen for our stent maps.

3.2 TAVI in a nutshell

The underlying pathological mechanisms of aortic valve stenosis results from a narrowing of the valve due to calcified leaflets. This implies that the blood has to be ejected against increased resistance. Additionally, abnormal high-velocity jets occur, which favor aneurysm development [4]. Aortic regurgitation can occur accompanying due to an insufficient closure of the leaflets. As a consequence, the blood pressure in the left heart and the lungs increases, causing a thickening and stiffening of the heart muscle [22]. Resulting symptoms are shortness of breath and chest pain.

The standard treatment for aortic valve stenosis according to actual guidelines [29] is the surgical implantation of a prosthetic aortic valve (example shown in Fig. 2b) necessitating the use of a cardiopulmonary bypass machine (CPB) and temporary cardiac arrest. Since 2002, a minimally-invasive alternative, the *transcatheter aortic valve implantation (TAVI)* exists. Instead of open surgery, the pathological aortic valve is approached with a catheter either via the aorta (retrograde) through access in the groin or via the left cardiac ventricle (anterograde) through the apex of the heart. A stent containing the prosthetic aortic valve is inserted, positioned, and released. The stent (which is either self-expandable or expanded with a balloon) pushes the degenerated native aortic valve against the aortic annulus, the prosthetic valve is unfolded, and takes over the valve function (see Fig. 2c). During this procedure, the interventionalist navigates in the heart by

means of transesophageal echocardiography (TEE) and CT angiography.

In the last eleven years, about 50.000 TAVI procedures were performed in more than 40 countries [23]. However, postoperative complications such as left bundle branch block (LBBB; may lead to cardiac arrhythmia) and transvalvular and paravalvular leakages are described [17]. In this paper we mainly address paravalvular leakages (PVL) describing the backflow of blood between the aortic wall/aortic annulus and the stent into the left cardiac ventricle during diastole. Five severity codes are distinguished: none, trivial, mild, moderate, and severe PVL [23].

PVL occurs when the stent does not completely attach to the surrounding structures leaving gaps for paravalvular blood flow. Several causes for an incomplete attachment are conceivable: (1) stent diameter too small for the patient's aortic annulus, (2) stent implanted too high so that blood flows past the prosthetic aortic valve through the stent, (3) stent implanted too low, which is problematic since the diameter at the stent's neck is smaller, (4) aortic valve stent not fully expanded, (5) amount and uneven distribution of calcifications located in the gap between stent and aortic wall.

In severe PVL cases, usually one of the following therapies is chosen: a further dilatation of the valve prosthesis with a balloon, the closing of the leakage hole with an occluder device or – if the valve prosthesis is implanted too low – the treatment with a second, higher implanted prosthesis (valve-in-valve) [27]. Since TAVI patients are mainly high-risk patients, each of these additional interventions is avoided if possible. Therefore, weaker PVL are usually not directly treated but closely monitored. Still, a higher one-year mortality has

been shown even with non-severe PVL [26]. The long-term goal of our project is to help prevent PVL by simulating TAVI procedures pre-operatively and giving the interventionalist advice on the best configuration regarding valve type and positioning. The intermediate goal is to be able to interpret simulation results and use them to predict PVL risks.

4 METHODS

In this paper, we present a visualization approach that incorporates relevant information about stent shape, radial forces, calcifications, anatomical situation etc. in a comprehensive 2D map representing the unrolled 3D scene. Without the necessity for an animated, interactive visualization of a 3D model on a computer screen, it allows to easily grasp the anatomy of the aortic valve, its spatial relation to the stent, and the amount and distribution of calcifications at one glance.

4.1 Requirements and design choices

To be useful for medical research, our visualization needs to meet the following requirements: First, it should communicate important *spatial relationships*. More specifically, it should clearly depict the patient’s individual anatomy of the aortic root (the shape of three sinuses/cusps, position of left and right coronary arteries), the amount and positions of calcium on the aortic valve, and the shape and relative position of the stent in the aortic root. Second, our system should display *multiple quantitative parameters*, such as the estimated radial forces, stent compression, and calcium thickness. Third, it should allow an *easy comparison of several datasets* in order to allow to identify patterns typical for cohorts with or without postoperative PVL. And fourth, the visualization approach should provide the basis for further *statistical analyses* and computational pattern matching.

To meet the requirements regarding comparability, we chose to transform the 3D data into 2D side-by-side visualizations (*stent map*) by virtually flattening the data. As an alternative approach, we considered connected 3D renderings of the different stent datasets, which would provide users with corresponding views on the different datasets while navigating. However, navigation is always necessary to view the important spatial aspects of the data, which makes it more difficult and time-consuming to get an overview. For this reason, we preferred the 2D version.

The area of the 2D map covers the area of the straightened and uncoiled stent. The map’s vertical axis corresponds to the (bent) centerline of the stent and the map’s horizontal axis corresponds to the angle around the centerline, like in a cylindrical coordinate system. The map itself is designed similar to a heatmap, i.e., it is constructed of tiles showing a quantitative property by color. Each tile contains the specific information of a 3D segment as seen from the stent’s centerline. By arranging several maps side-by-side, we fulfill the requirement to show multiple parameters. Here, we considered the alternative to display more than one quantitative parameter per map by color-mixing or by encoding more than one property per tile with an approach as shown in [12]. However, we chose the side-by-side version, since a complex encoding strategy would decrease comprehensibility and complicate pattern identification for the users. A redesign in this regard might be useful as soon as the relevant properties are identified and it is clear what users must be looking for in these maps.

Finally, we communicate spatial relationships and important anatomical information with graphical markups that are drawn on the map, similar to the borders between countries on a geographical map. The following structures are depicted by these markups: (1) the shape of the aortic valve and the ostia of the coronary arteries from the aortic root, (2) the contours of the calcifications as segmented from the CT data, and (3) the stent contours. These stent contours together with the color-coded stent distortion (see Sec. 4.3.2) display the necessary information about the stent shape.

4.2 Data preprocessing and mechanical analysis

The process of postoperative CT image acquisition, the method for extracting information about the postoperative stent shape from these images and how that information is used in a mechanical analysis to

create an estimate of the radial forces between the stent and the surrounding tissues and calcifications is presented in [9] and [10]. Here, we confine ourselves to a brief overview over these techniques, and refer the reader to the cited papers for further detail.

We obtained CT images (see Fig. 2a) from patients who had received a self-expandable TAVI prosthesis (see Fig. 2b). A set of landmarks is automatically extracted from those images, which represent the intersection points, or grid points, of the stent’s mesh structure, using some diligence to separate the stent from the surrounding calcifications, which show a similar intensity in the images. A mechanical model of the stent in its original (undeformed) shape was created from microCT scans of the device and a method for using the grid points extracted from the patient images as soft kinematic constraints was developed [14]. In [10] we describe, how this method is used to simultaneously reduce point localization errors that occur during the localization of the grid points and to extract estimates for the radial force between the stent and its surroundings. The basic idea here is to derive the radial forces from the deformation of the implanted stent when compared to the relaxed stent shape.

For the presented approach, two additional manual processing steps were added to the pipeline as described in [10]: (1) With an expert clinician, six anatomical landmarks at the aortic annulus (the three commissures and the three sinuses) as well as the approximate position of the left and right coronary arteries were marked manually in the CT images (see Fig. 2a). (2) After subtracting the, now known, stent from the CT images, the remaining high-intensity voxels near the aortic root are considered calcium. Morphological operators are employed to erase very small bits of calcium (by morphological opening) and to close very small holes in larger chunks of calcium (by morphological closing) before computing surface models of the calcifications.

4.3 Map creation

After the previously described preprocessing steps, the relevant data are available as geometric meshes of stent (containing the radial force value for each vertex) and calcium as well as the eight anatomical landmark positions. In the following, the separate steps of map generation are described in more detail.

4.3.1 Generalized cylindrical coordinates

The area of the stent map corresponds to the area of the straightened and unrolled stent (seen from the inside). Thus, to draw the map, the mesh positions and its parameters need to be assigned to the respective map locations. This can be considered as a cylindrical mapping based on a curved cylinder around the stent. As a first step and in order to facilitate this mapping, we transform our 3D scene from cartesian to the stent’s cylindrical coordinates. For this, we generate the stent model’s centerline and determine for each vertex in the scene the cylindrical coordinates with respect to this centerline. More specifically, in its undeformed shape, the stent can be very well described in cylinder coordinates defined around its central axis. To allow for a similar representation in a deformed shape, where the centerline of the stent can be (slightly) bent, we rely on a *generalized definition of cylindrical coordinates* (see Fig. 4b):

For a given, not necessarily straight, C^1 -smooth curve $\mathbf{c} : [a, b] \rightarrow \mathbb{R}^3$ and a reference point $\mathbf{q} \in \mathbb{R}^3$, generalized cylinder coordinates (r, α, h) of a cartesian point $\mathbf{p} \in \mathbb{R}^3$ with respect to \mathbf{c} are defined as follows:

- The height h is defined by the arc length computed along the curve \mathbf{c} from its origin $\mathbf{c}(a)$ to the orthogonal projection \mathbf{p}_c of \mathbf{p} onto \mathbf{c} .
- The radius $r = \|\mathbf{p}_c - \mathbf{p}\|$.
- The angle α is defined by the angle between \mathbf{p} and the projection \mathbf{q}_p of \mathbf{q} onto a plane \mathbf{E} orthogonal to \mathbf{c} in \mathbf{p}_c , measured around the central point \mathbf{p}_c .

The construction requires the curvature of \mathbf{c} to be reasonably low to ensure that the orthogonal projection of each \mathbf{p} onto \mathbf{c} is definite. This

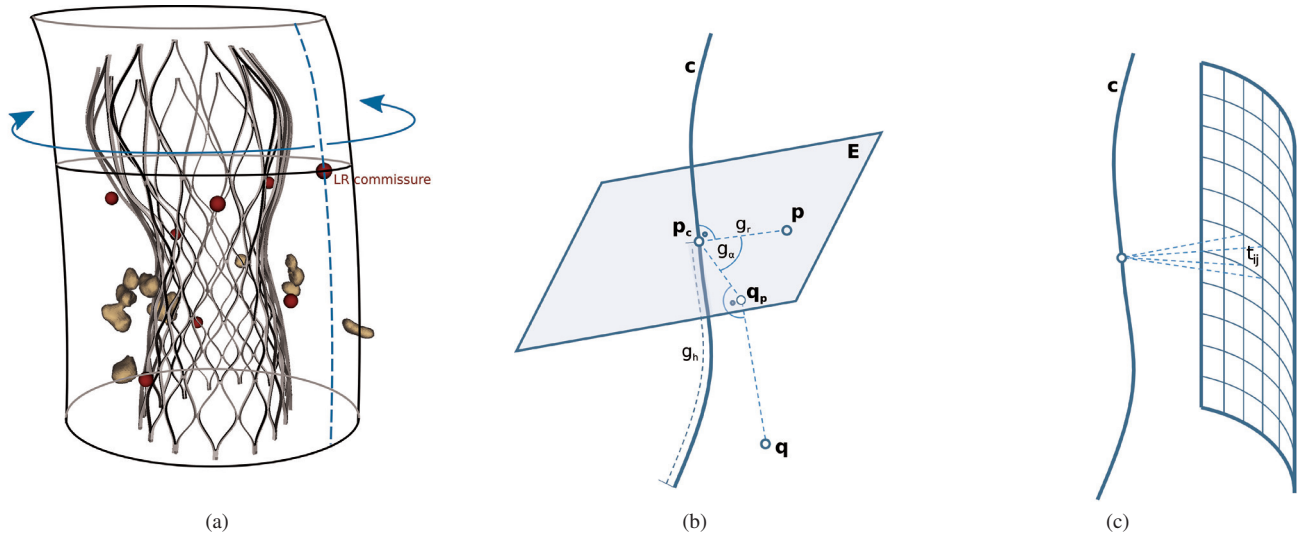


Fig. 4. (a) Generalized cylinder wrapped around the deformed stent. The datasets are cut and unrolled at a consistent landmark. (b) Construction of generalized cylinder coordinates. (c) Map tile on the surface of the generalized cylinder.

curvature requirement is fulfilled in our case, since the implanted aortic valve stents are compressed but not strongly bent. As reference point, we use the commissure between the left and right coronary sinus (see arrow in Fig. 1a). This commissure therefore corresponds to an angle of 0° and represents the left and right border of the stent map.

As a result of this step, a specific position in the 3D scene can be mapped to a specific position in the 2D stent map (i.e., a specific tile). More specifically, the angle of the generalized cylindrical coordinates corresponds to the horizontal axis and the height to the vertical axis in the map. We further speed up the processing by binning the mesh vertices according to height and angle of these generalized cylindrical coordinates.

4.3.2 Creating the map

The stent map consists of tiles. Each tile corresponds to a 3D segment of the scene as viewed from the stent's centerline (see Figure 4c) and its color represents the respective parameter value of this segment. The user can adjust the number of tiles in height and width and with that change the resolution from a high-resolution rendering of the scene (where a tile is simply represented by a pixel) to a more abstract heatmap with reduced data dimensionality.

As a next step in map creation, the respective parameter values for the tiles need to be computed. We implemented and compared two variants.

Direct vertex assignment The first variant is a straight-forward assignment of a vertex to the map tiles based on its generalized cylindrical coordinates. For each vertex $\mathbf{v} \in \mathbb{R}^3$, we use the following equations to compute the two-dimensional index (i, j) of its respective tile \mathbf{t}_{ij} :

- $i = \left\lfloor \frac{\mathbf{v}_\alpha}{\alpha_t} \right\rfloor$ with $\alpha_t = \frac{360^\circ}{n_w}$
- $j = \left\lfloor \frac{\mathbf{v}_h}{h_t} \right\rfloor$ with $h_t = \frac{h_s}{n_h}$

with the stent height h_s and the map resolution $n_w \times n_h$.

As explained previously in Section 4.1, the different parameters of interest for each tile are the radial force \mathbf{rf} , the calcium thickness \mathbf{ct} , and the stent compression \mathbf{sc} . We compute a tile's \mathbf{rf} by determining the maximal radial force over all stent mesh vertices assigned to this tile. We compute a tile's \mathbf{ct} by subtracting the minimal from the maximal radius of calcium mesh vertices assigned to this tile. As only calcium in the closer vicinity of the stent is of interest, we neglect the calcium information for a tile with a minimal calcium radius larger

than 6 mm . Finally, for the computation of a tile's \mathbf{sc} , we determine the tile's maximal, absolute difference of stent radius to the original radius r_{orig} of the unimplanted stent at the same height. The stent compression is then determined by $\mathbf{sc} = \frac{r - r_{orig}}{r_{orig}}$.

The advantage of this method is its efficiency and low run-time. However, it also introduces inaccuracies since only vertex information not triangle information is used for map creation (see further discussion in Sec. 5.3, 6).

Therefore, we also implemented a more precise sampling method that we will compare this method to.

Raycasting The second variant is a raycasting, which samples the 3D scene with rays capturing one 3D segment each. Rays are started from the stent's centerline and capture the scene orthogonal to the centerline in equal angular steps. The resulting map shows the 3D scene from the stent's inside and implicitly straightens the scene. This raycasting approach can be efficiently implemented by utilizing the generalized cylindrical coordinates. The direction of a ray can be given by an angle and height in generalized cylindrical coordinates. Checking for an intersection of a ray with a triangle then boils down to checking whether a 2D point lies in a 2D triangle. Instead of rendering the illuminated mesh (as with traditional raycasting), the properties of maximal radial forces, stent compression, and minimal and maximal calcium radius are determined like in the previous section and stored for each ray for further processing. For each ray, all triangles in the bin need to be tested. The number of rays is not determined by the map or screen resolution but chosen so that the scene is sufficiently sampled. Therefore, we use a virtual resolution of 2400×1200 . This means that a ray covers a 3D segment of 0.15° and a height of about 0.04 mm (stent height ranges between 51.15 mm and 53.87 mm). From this potentially oversampled information, the map with the user-desired tile resolution is determined by aggregating ray information and determining the respective maximal radial force, calcium thickness, and stent compression for the tile.

Due to the stent's grid-like shape, the stent data (necessary for stent compression and calcium thickness properties) in the map is only sparse. With both sampling methods, the missing information between the stent wires is linearly interpolated from the neighboring stent information for complete coverage.

Context rendering

The anatomical and stent context is displayed in the map as a spatial guide for the users. It allows them to detect patient-specific aortic

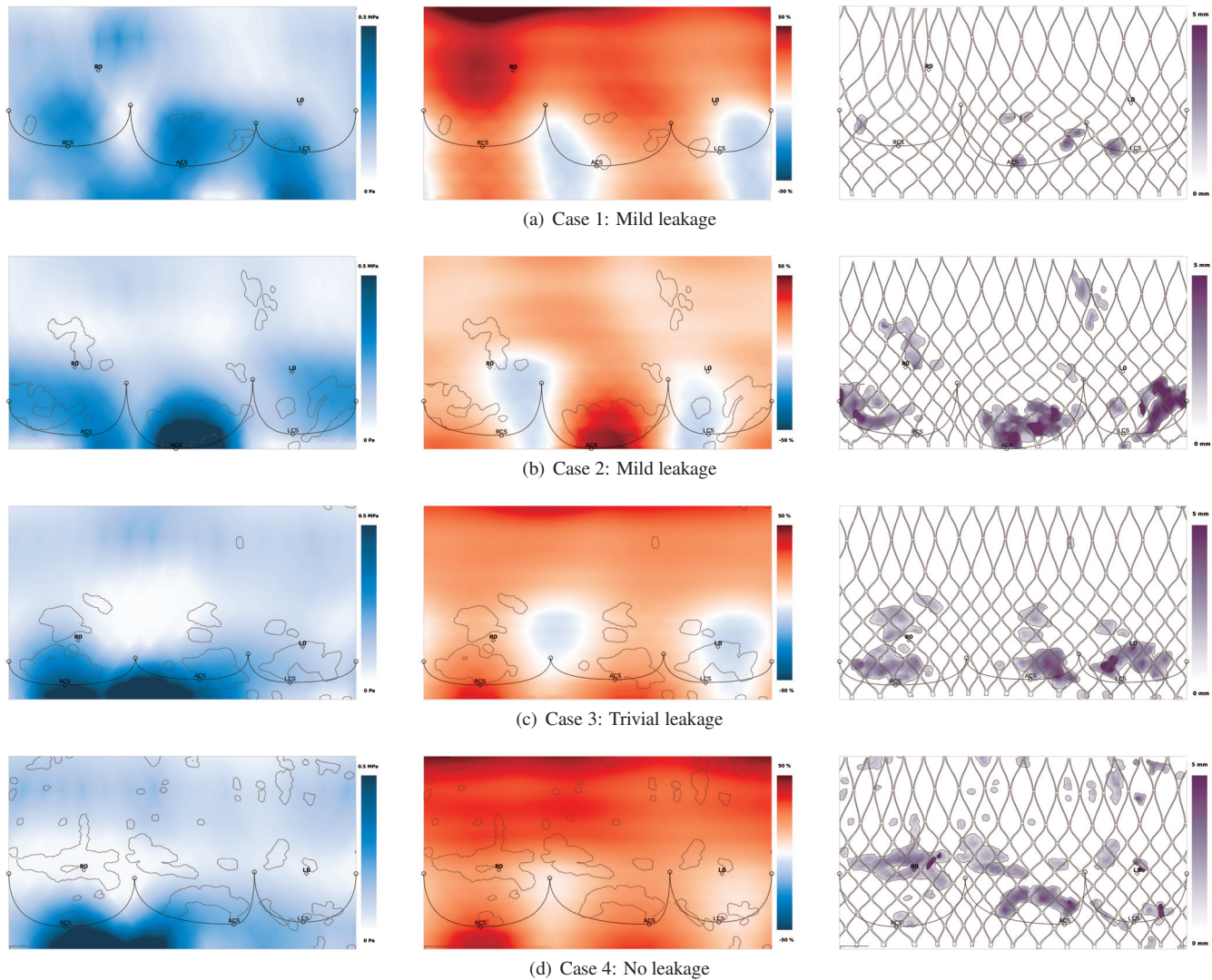


Fig. 5. Stent maps of four TAVI patients (one patient per row). Each column shows a different parameter of interest. Left: Radial force. Middle: Stent compression (red indicates compression, blue expansion with respect to original stent shape). Right: Calcium thickness. All color maps in a column are scaled equally. Abbreviations: Left coronary artery (LA), right coronary artery (RA), left coronary sinus (LCS), right coronary sinus (RCS), non-coronary sinus (ACS).

valve anomalies, analyze the stent implantation height, stent deformation, amount and distribution of calcium, and to rate the different map parameters in this context. In order to avoid the occlusion of the color-coded map parameters, all context is displayed as an unobtrusive, comprehensible line rendering.

The anatomical landmarks, which were detected in the CT data previously (see Sec. 4.2), are now used to render the patient-individual shape of the aortic valve (similar to Fig. 1b). The localization of the landmarks on the stent map is done analogously to the direct vertex assignment by using generalized cylindrical coordinates. The valve crown is defined by the three commissure landmarks and the three bottom points of the sinuses. From these six landmarks the crown-shape is approximated with one B-spline curve per sinus. Further, the left and right coronary arteries are displayed and annotated.

The calcifications are shown as contours of the calcium chunks. These contours are drawn at the borders of tiles with and without calcium information. This implies that the calcium renderings have the same resolution as the complete stent map and appear unsmooth for lower resolutions. The stent contours can be rendered analogously to the calcium context.

Population stent maps

It is not only of interest to analyze data of individual patients, but also of larger populations. For this matter, we generate population stent maps providing results of statistical evaluations (as, e.g., mean, standard deviation, weighted differences) conducted on the parameter data of patient cohorts with or without PVL. The anatomical landmark positions are averaged for each cohort and displayed as its mean aortic valve morphology. Altogether, these population maps allow to detect typical patterns for leaking and leakproof cases and to compare the individual patient to these patterns.

5 RESULTS

We applied our stent map technique to 15 postoperative CT datasets of TAVI patients (3 cases without leakage, 4 cases with trivial leakage, 8 cases with mild leakage, no cases with moderate or severe leakage). Figure 5 shows exemplary results for four patients with different PVL outcomes. These maps display several patient-individual anatomical aspects and spatial information about the implanted stent: From the arch-like sinus renderings, one can observe distinctive anatomical features like, e.g., the rather flat aortic root in case 3 (see narrow arches in Figure 5c). The height of the sinus renderings on the map reflects

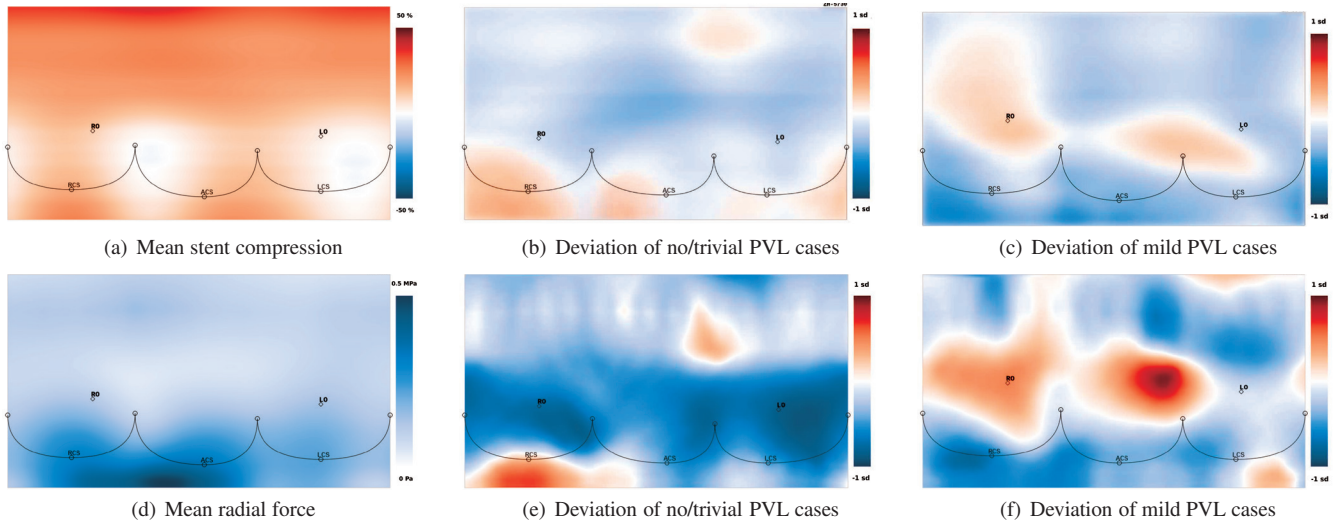


Fig. 6. Population stent maps for stent compression (top row) and radial forces (bottom row). The left column shows the map with the parameter mean for all 15 datasets. In (a) the elliptical shape of the stent profile can be observed. (d) shows the maximal force concentration on the bottom left border of the stent maps. The middle column shows the difference of the parameter mean of the whole population and the no/trivial leakage cohort weighted with the standard deviation (sd). The right column shows the same for the mild leakage cohort. The color maps in b,c,e,f have the same scale. Abbreviations: Left coronary artery (LA), right coronary artery (RA), left coronary sinus (LCS), right coronary sinus (RCS), non-coronary sinus (ACS).

the stent implantation height. Highly-positioned sinuses in the map correspond to a low implantation (see Fig. 5a), and vice versa (see Fig. 5b). The shape of the implanted stent is shown by the stent overlay (see Fig. 5, right column) and the color-coded stent deformation (Fig. 5, middle column). The calcium contour renderings and the calcium thickness map (Fig. 5, right column) allow conclusions regarding the amount and distribution of calcifications in the vicinity of the stent. From the radial force maps (Fig. 5, left column) one can study maximal or minimal force values and their distribution. Finally, population maps (see Fig. 6) show the same criteria for larger patient subgroups and allow researchers to identify patterns typical for different PVL outcomes.

5.1 Feedback of clinical experts

We introduced our method to two heart surgeons (co-authors; one very experienced, one assistant physician) separately by showing and explaining 2-3 stent maps and giving them the opportunity to also explore the corresponding postoperative CT data (similar to Fig. 2a) and 3D stent visualizations with embedded landmark positions and calcifications (similar to Fig. 3). After that, they analyzed the 15 datasets with known PVL outcome. The goal of this overall procedure was to observe the experts during training and analysis and collect their feedback about the visualization, but at the same time to start generate strategies to predict PVL from these maps (by pattern identification).

Heart surgeons are used to work with CT image data, which is mainly viewed as 2D slices (see Fig. 2a). Surgeons are well-trained in mentally creating a three-dimensional impression of this 2D data. However, stent maps show a different kind of 2D view the experts are not used to. Consequently they needed some training to understand and translate the 2D stent map into a mental 3D model as well. The training helped them understand the shown view point, the order of the sinuses, and the color-codings (especially the deformation map). Still, the training phase took no longer than 10 min during which they already started to discuss similarities and differences in the maps and possible conclusions.

Preliminary medical insights gained from these analyses are described in Section 5.2. During analysis, they appreciated the design decision to rely on several side-by-side maps with consistent layout instead of trying to create an all-in-one visualization at this state. Altogether, this design facilitated to grasp the characteristics of one dataset by exploring its numerous parameters and to compare these charac-

teristics in different datasets with different outcomes. At a glance, it was possible for them to identify cases with, e.g., especially high or low positioned stents, with concise force maxima or especially thick and unevenly distributed calcifications. They stated that this would not be possible with state-of-the-art 3D visualizations of the same CT and simulation data (see Fig. 3). These are appropriate for a 3D spatial impression of a single dataset but have several disadvantages: (1) It takes longer to get an overview over a single dataset due to the necessary navigation; (2) comparison of several datasets is more difficult because users need to repeatedly orientate themselves in the anatomy (e.g., identify the sinuses) and find corresponding landmarks; (3) one cannot easily quantify and compare parameters like deformation or calcium distance to the stent, which is possible with the color-coded parameter values in the stent maps; (4) 3D visualizations of whole populations are also not available. So, altogether, the heart surgeons appreciated the advantages of this visualization and are confident that this research direction will bring interesting insights when applied to a larger database.

Further, the clinical experts could imagine several variants and other use cases for this visualization technique. It could easily adapted to other heart valve interventions like the catheter-based implantation of pulmonary or mitral valve prostheses. These are not clinically established yet, but similar questions about selecting the most appropriate valve type, size, and position will come up and the adaption of stent maps to other anatomical situations and prostheses types is rather straight-forward. Other interesting use cases is the planning of different types of aneurysm stenting. A suitable cardiovascular example is the endovascular aneurysm repair (EVAR). Here, Y-shaped stents are inserted minimally-invasive to treat aneurysms in the abdominal aorta. Complications of interest are endoleaks (where an aneurysm is still supplied with blood) or the blocking of important branching arteries. The anatomical situation is comparable between patients and therefore well-suited for analysis with stent maps. Also thinkable is the addition of blood flow information from CFD simulations or flow-sensitive MRI measurements. A second aneurysm use case could be the planning of flow diverter stenting of cerebral aneurysms. Here, complications like stent creeping or perforator infarctions (where the blood flow in important branching vessels is pathologically altered) are investigated. Apart from vessel stenting, tracheal or oesophageal stenting could be investigated as possible stent map applications. Altogether, it is thinkable to adapt and apply stent maps to several other

medical use cases and maybe even establish it as a standard way of displaying multi-parametric data in these contexts (similar to the bull's eye plot described in Sec. 2).

As limitations the medical experts stated the uncertainty about the landmarks. These are reconstructed from the underlying CT data and thus depend on experts' manual positioning. However, this drawback is also true for CT data and the previously shown 3D visualizations. Further, they missed interactivity. In contrast to computed tomography series where the clinician can scroll through the layers, the expert only has one set of images with a lower degree of interaction at his disposal. However, they could not state in detail what further interactions they needed.

As result from this feedback, we believe that an increased acceptance of this visualization method can be expected by training them with typical and representative example cases and by making additional CT data and 3D visualizations available, so that they can – when in doubt – double-check the data with familiar display techniques. Acceptance in clinical routine should also be increased by further research, i.e., when more patterns and criteria have been found for different outcomes, the clinicians will know what they are looking for. When that state of maturity will be reached in the future, they would also vote for a more compact display for use in the clinical routine, i.e., when risk factors for PVL are better known and the visualization would serve not for pattern searching but to merely display simulation results. Then, it might also not be of great importance anymore to create an anatomical mental model from the stent maps but to check for known patterns in rather abstract images.

5.2 Medical insights

Several interesting medical insights have been gained from the stent map visualizations. These insights are preliminar until a larger number of cases has been analyzed, but still very promising.

- Not the mere presence or absence of calcium seems to be important for PVL occurrence, but calcium distribution: mild leakage case 1 has PVL but only very little calcifications, whereas case 4 (without leakage) has lots of calcium but no PVL. For example, it is thinkable that neighboring, thick calcium chunks (see Fig. 5b) form a channel for the blood to flow through. Especially if at the same position the radial force is low and/or the stent is not very compressed.
- From the radial force maps a force concentration at the stent map's lower end below RCS and NCS can be observed for cases 3 and 4. The PVL cases 1 and 2 differ from this pattern. Especially case 1 shows rather low overall force, which might cause PVL because the stent does not sufficiently adapt to its surrounding structures (because it is not fully expanded or the chosen stent size is too small).
- The mild leakage cases 1 and 2 show comparably low and comparably high implantation heights respectively. Cases 3 and 4 with trivial and no leakage, however, have well-positioned stents. This might confirm the theory that an inappropriate implantation height has a strong influence on PVL occurrence.
- A very interesting observation are two blueish stripes in the stent compression maps (middle column) – with one of the stripes located very close to the RN-commissure. The oval shape of the implanted stent (which is the meaning of the stripe pattern) has been observed before but it is a new finding that the oval shape seems to have a preferred orientation in the aortic annulus. The mean stent compression over all 15 patient datasets is shown in Figure 6a and also clearly displays the elliptical shape observed with the four datasets in Figure 5.
- When comparing stent compression data of cohorts of similar outcomes to the mean data, deviations can be noticed: the mild leakage cohort (see Fig. 6c) shows lower compression at the lower end of the stent and higher compression in the middle region; the cohort of non-leakage and trivial leakage cases (which

we examine as one population) shows almost the inverted pattern with more compression in the area below the RCS and less compression above the aortic valve.

- A similar pattern difference can also be observed for the radial force information. Figure 6d shows the mean force of the whole population. The maximum force concentration below RCS stands out clearly, which is lowered in the mild leakage cohort (see Fig. 6f) and even stronger in non-leakage and trivial cases (see Fig. 6d).

The mean force and compression patterns are very interesting findings for the clinical experts, as they give a hint on possible PVL prediction patterns. However, these deviation patterns are observed in a study of only 15 datasets. Therefore, they will be further applied to a larger population in the future and hopefully confirm the tendency that the cohorts can be distinguished with this approach.

5.3 Comparison of sampling methods

The advantage of sampling with raycasting is its precision, which however comes at the cost of some preprocessing time (for sampling and interpolation). The actual map drawing (tile averaging and rendering) depends on the map resolution and takes below 250 ms for a lower tile resolution (120 × 70) and 345 ms – 975 ms for a higher tile resolution (1000 × 600). The different times relate to different parameters with different processing costs. The preprocessing may take up to 10s. However, it could be decreased by code optimization and by using a smaller number of rays.

With direct vertex assignment (DVA) the scene is sampled whenever the map is rendered, which makes preprocessing unnecessary. For a larger tile resolution the map creation (which includes sampling, interpolation, and rendering) takes slightly longer than the raycasting method (between 850 ms and 1.21 s) and has the disadvantage that holes occur when triangles are larger than the tiles (because only vertices are mapped, not the triangles). For smaller resolutions however the run-time is considerably lower than the raycasting method (below 22 ms).

For comparative visualization, we don't necessarily aim at highly resolved images but rather at small multiple views so many maps fit on the screen for comparison. For this, a lower map resolution is sufficient and the cheaper vertex assignment is a valid alternative provided that it is accurate enough. The maps produced by DVA are visually comparable to raycasting. An additional quantitative comparison of these maps was conducted by analyzing the normalized root mean square errors (NRMSE), which produced a low mean NRMSE (over all datasets combined) of 0.06 for force and compression maps and 0.04 for calcium thickness maps. The NRMSE for the individual datasets is given in Figure 7.

Following these analyses, we use the faster DVA for small multiples generation, but still rely on raycasting when we generate data for statistical analyses or high-quality images (as shown in the previous section). Further, one needs to keep in mind that the map accuracy not only depends on the sampling but also on the interpolation technique, which we will further research in the future (see Sec. 6).

6 CONCLUSION

In this work, we have presented stent maps, which are a multi-parametric visualization of medical CT data and mechanical simulation results. This tool is applied for the research of indicators for PVL occurrence after TAVI. Stent maps represent the area of the unrolled stent and show aortic valve anatomy, calcifications, and stent shape as line renderings. The parameters of interest, which are suspected to have an influence on the occurrence of PVL, are shown in a heatmap-like manner. With that, stent maps incorporate all information of interest in a comprehensible way and allows a convenient overview over different parameter patterns of individual patients and patient cohorts. This compact information integration is not achieved when viewing the data as 3D scene or examining the raw CT data and therefore could improve the planning of TAVI procedures. The resolution of the map can be adjusted from a highly-resolved view with a

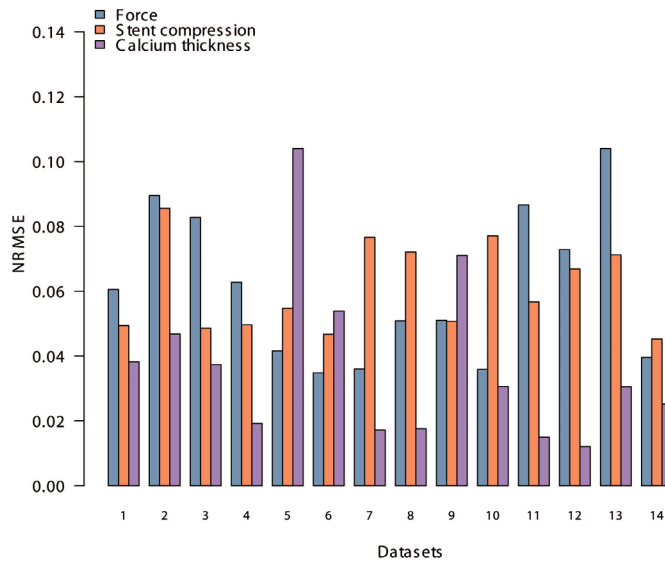


Fig. 7. Comparison of maps rendered with raycasting or by assigning vertices directly to the tiles. (a) Diagram shows the normalized root mean square error (NRMSE) of the maps for the 15 datasets for each parameter map separately.

higher image quality to a low-resolution, more abstract version. The latter is useful for view as small multiples and if a larger dimensionality reduction is desired for further statistical or computational analysis.

For the local assignment of mesh data onto a stent map, we have implemented two sampling methods differing in run-time. Comparison of stent maps rendered with the two methods showed that for lower-resolved images the direct vertex assignment and the raycasting method achieve results with comparable quality. Therefore, the faster DVA method is valid for use with the small multiples view.

The application of our method to 15 datasets revealed several novel radial force and stent compression patterns, which are very promising to bring clinical research closer to understanding different risk factors and their interaction in the context of PVL formation. The gained insight confirms that the abstraction and dimensionality reduction of our method helps comparing numerous datasets and finding patterns, which has not been feasible with other methods, such as 3D renderings as shown in Figure 3. The clinical experts are confident that we will yield significant results when applying our methods of mechanical simulation and stent maps to a larger database. Also, the application of stent maps to other medical use cases such as the preoperative planning of other heart valve interventions or aneurysm stenting could be very beneficial.

Our work gives several starting points for future work. The first has been mentioned already, which is the extension of our training database regarding the number of datasets and types of leakage severities (moderate and severe PVL missing so far). When doing so, new requirements or new parameters of interest might arise. Further, the patterns we have found were eye-catching in the sense that they could also help explain the occurrence of other side effects such as transvalvular leakages and left bundle branch block. Therefore, an investigation considering these outcomes would be of great medical interest as well. A further important aim is the translation of these new tools into clinical practice by facilitating and accelerating the methods necessary to create the stent maps. From a technical point of view, we plan to not only rely on human pattern matching abilities, but we will intensify our research with machine learning and computational pattern matching. Also, the linear interpolation scheme we used for the approximation of stent distances and radial forces between the stent wires is very simple. It has shown satisfactory results, but especially for the forces, we will check whether a more sophisticated interpolation method (such as, e.g., spatial kriging) is more appropriate. Further, we want to investi-

gate whether the strict cut-off at one commissure hinders identifying patterns stretching over this landmark. Alternatively, one could repeat a portion of the neighboring sinus at both ends of the map. A mentioned limitation of our approach is the uncertainty of the manually defined landmarks. We will work on an appropriate way of communicating this uncertainty in the individual and the population stent maps. Finally, we have decided to use a side-by-side visualization approach for the sake of clarity and comprehensibility. For the future, when patterns and PVL indicators are more clear, the goal will be to create a more compact visualization of standardized patterns hinting on PVL occurrence, which would further improve usability for the expert clinician.

ACKNOWLEDGMENTS

The authors wish to thank Stefan Schwyter for preparing the medical illustrations. This work was supported in part by the Swiss National Science Foundation (grant no. CR3213_135044).

REFERENCES

- [1] P. Angelelli and H. Hauser. Straightening tubular flow for side-by-side visualization. *IEEE TVCG*, 17(12):2063–2070, 2011.
- [2] L. Antiga and D. Steinman. Robust and objective decomposition and mapping of bifurcating vessels. *IEEE T Med Imaging*, 23(6):704–713, 2004.
- [3] F. Auricchio, M. Conti, S. Morganti, and A. Reali. Simulation of transcatheter aortic valve implantation: a patient-specific finite element approach. *Comput Method Biomec*, (March 2013):37–41, Feb. 2013.
- [4] A. J. Barker, M. Markl, J. Bürk, R. Lorenz, J. Bock, S. Bauer, J. Schulz-Menger, and F. von Knobelsdorff-Brenkenhoff. Bicuspid Aortic Valve is Associated with Altered Wall Shear Stress in the Ascending Aorta. *Circulation*, 5(4):457–66, July 2012.
- [5] A. V. Bartoli, R. Wegenkittl, A. König, and E. Gröller. Nonlinear virtual colon unfolding. In *IEEE Visualization*, pages 411–420, 2001.
- [6] C. Capelli, G. M. Bosi, E. Cerri, J. Nordmeyer, T. Odenwald, P. Bonhoeffer, F. Migliavacca, a. M. Taylor, and S. Schievano. Patient-specific simulations of transcatheter aortic valve stent implantation. *Med Biol Eng Comput*, 50(2):183–92, Feb. 2012.
- [7] S. Diepenbrock, S. Hermann, M. Schäfers, M. K. And, and K. Hinrichs. Comparative Visualization of Tracer Uptake in In Vivo Small Animal PET/CT Imaging of the Carotid Arteries. *Comput Graph Forum*, 32(3):241–250, 2013.
- [8] FEops (Gent, Belgium). FEops – Better healthcare through simulations, Mar. 2014.
- [9] M. Gessat, L. Altwegg, T. Frauenfelder, A. Plass, and V. Falk. Cubic hermite bezier spline based reconstruction of implanted aortic valve stents from ct images. In *Proc. of IEEE EMBC*, pages 2667–2670, Aug 2011.
- [10] M. Gessat, R. Hopf, T. Pollok, C. Russ, T. Frauenfelder, S. Sündermann, S. Hirsch, E. Mazza, G. Szekely, and V. Falk. Image-based mechanical analysis of stent deformation: Concept and exemplary implementation for aortic valve stents. *IEEE T Bio-Med Eng*, 61(1):4–15, Jan 2014.
- [11] O. Gjesdal and T. Edvardsen. Tissue Doppler in ischemic heart disease. *Establishing better standards of care in Doppler echocardiography, computed tomography and nuclear cardiology*, 2011.
- [12] S. Glaß er, U. Preim, K. Tönnies, and B. Preim. A visual analytics approach to diagnosis of breast DCE-MRI data. *Computers & Graphics*, 2010.
- [13] K. Gurijala, R. Shi, W. Zeng, X. Gu, and A. Kaufman. Colon Flattening Using Heat Diffusion Riemannian Metric. *IEEE TVCG*, 19(12):2848–2857, 2013.
- [14] R. Hopf, G. M., F. V., and M. E. Reconstruction of stent induced loading forces on the aortic valve complex. In *Proc. of MICCAI-Workshop on Computer-Assisted Stenting*, pages 104–111, October 2012.
- [15] T. Huysmans, J. Sijbers, and B. Verdonk. Parameterization of Tubular Surfaces on the Cylinder. *Journal of WSCG*, 13(3):97–104, 2005.
- [16] A. Kanitsar, R. Wegenkittl, D. Fleischmann, and M. Groller. Advanced curved planar reformation: flattening of vascular structures. *Proc. of IEEE Visualization*, pages 43–50, 2003.
- [17] S. K. Kodali, M. R. Williams, C. R. Smith, L. G. Svensson, J. G. Webb, R. R. Makkar, G. P. Fontana, T. M. Dewey, V. H. Thourani, A. D. Pichard, M. Fischbein, W. Y. Szeto, S. Lim, K. L. Greason, P. S. Teirstein, S. C. Malaisrie, P. S. Douglas, R. T. Hahn, B. Whisenant, A. Zajarias, D. Wang,

- J. J. Akin, W. N. Anderson, and M. B. Leon. Two-year outcomes after transcatheter or surgical aortic-valve replacement. *New Engl J M*, 366(18):1686–95, May 2012.
- [18] D. Lindahl, J. Palmer, J. Pettersson, T. White, A. Lundin, and L. Edénbrandt. Scintigraphic diagnosis of coronary artery disease: myocardial bull’s-eye images contain the important information. *Clin Physiol*, 18(6):554–561, 1998.
- [19] M. Minoves, A. Garcia, J. Magrina, J. Pavla, R. Herranz, and J. Setoain. Evaluation of myocardial perfusion defects by means of bulls eye images. *Clin Cardiol*, 22:16–22, 1993.
- [20] G. Mistelbauer, A. Morar, A. Varchola, R. Scherthner, I. Baclija, A. Kéchl, A. Kanitsar, S. Bruckner, and E. Gröller. Vessel Visualization using Curvicircular Feature Aggregation. *Comput Graph Forum*, 32(3):231–240, 2013.
- [21] M. Neugebauer, R. Gasteiger, O. Beuing, V. Diehl, M. Skalej, and B. Preim. Map Displays for the Analysis of Scalar Data on Cerebral Aneurysm Surfaces. *Comput Graph Forum*, 28(3):895–902, June 2009.
- [22] R. Nishimura. Aortic Valve Disease. *Circulation*, 106(7):770–772, Aug. 2002.
- [23] C. Reidy, A. Sophocles, H. Ramakrishna, K. Ghadimi, P. Patel, and J. G. T. Augoustides. Challenges after the first decade of transcatheter aortic valve replacement: focus on vascular complications, stroke, and paravalvular leak. *J Cardiothorac Vasc Anesth*, 27(1):184–9, Feb. 2013.
- [24] T. Ropinski, S. Hermann, R. Reich, M. Schäfers, and K. Hinrichs. Multimodal vessel visualization of mouse aorta PET/CT scans. *IEEE TVCG*, 15(6):1515–22, 2009.
- [25] C. Russ, R. Hopf, S. Hirsch, S. Sündermann, V. Falk, G. Szekeley, and M. Gessat. Simulation of transcatheter aortic valve implantation under consideration of leaflet calcification. In *Proc. of IEEE EMBC*, pages 711–714, July 2013.
- [26] C. Tamburino, D. Capodanno, A. Ramondo, A. S. Petronio, F. Ettori, G. Santoro, S. Klugmann, F. Bedogni, F. Maisano, A. Marzocchi, A. Poli, D. Antoniucci, M. Napodano, M. De Carlo, C. Fiorina, and G. P. Ussia. Incidence and predictors of early and late mortality after transcatheter aortic valve implantation in 663 patients with severe aortic stenosis. *Circulation*, 123(3):299–308, Jan. 2011.
- [27] G. Tarantini, V. Gasparetto, M. Napodano, C. Fraccaro, G. Gerosa, and G. Isabella. Valvular leak after transcatheter aortic valve implantation: a clinician update on epidemiology, pathophysiology and clinical implications. *Am J Cardiovasc Dis*, 1(3):312–20, Jan. 2011.
- [28] M. Termeer, J. Oliván Bescós, M. Breeuwer, A. Vilanova, F. Gerritsen, and E. Gröller. CoViCAD: Comprehensive visualization of coronary artery disease. *IEEE TVCG*, 13(6):1632–9, 2007.
- [29] A. Vahanian, O. Alfieri, F. Andreotti, M. J. Antunes, G. Barón-Esquivias, H. Baumgartner, M. A. Borger, T. P. Carrel, M. De Bonis, A. Evangelista, V. Falk, B. Iung, P. Lancellotti, L. Pierard, S. Price, H.-J. Schäfers, G. Schuler, J. Stepinska, K. Swedberg, J. Takkenberg, U. O. Von Oppell, S. Windecker, J. L. Zamorano, and M. Zembala. Guidelines on the management of valvular heart disease (version 2012). *Eur Heart J*, 33(19):2451–96, Oct. 2012.
- [30] Q. Wang, E. Sirois, and W. Sun. Patient-specific modeling of biomechanical interaction in transcatheter aortic valve deployment. *J Biomech*, 45(11):1965–71, July 2012.
- [31] L. Zhu, S. Haker, and S. Tannenbaum. Flattening maps for the visualization of multibranch vessels. *IEEE T Med Imaging*, 24(2):191–198, 2005.